THE EFFECT OF THE DELTA WING VORTEX SYSTEM ON THE FLOW AROUND LIFTING SURFACES

© 2025 V. E. Borisov, T. V. Konstantinovskaya*, and A. E. Lutskii

Keldysh Institute of Applied Mathematics of the Russian Academy of Sciences, Moscow, Russia
**e-mail: konstantinovskaya.t.v@gmail.com*

Received January 20, 2025

Revised February 27, 2025

Accepted February 27, 2025

Abstract. The vortex structures formed behind a delta wing in supersonic flow are considered. The dependence of these structures on the angle of attack and the oncoming flow Mach number is studied, together with their effect on the aerodynamic properties of a downstream straight wing. The regimes with M = 2 and 3 and α = 10°, 14°, and 20° are considered. The numerical data are obtained using the hybrid multiprocessor supercomputer K-60 system in the Common Use Center of the Keldysh Institute of Applied Mathematics of the Russian Academy of Sciences.

Keywords: *supersonic flow, delta wing, vortex system of a delta wing, secondary vortices, aerodynamic parameters of a wing*

DOI: 10.31857/S10247084250310e8

INTRODUCTION

During the flight of high-speed aircraft, various vortex systems caused by lift-off on various structural elements tend to occur. Interacting with the hull, these vortices affect the overall performance, stability and controllability of the aircraft. Depending on the shape of the aircraft and flight regimes, vortices can be very complex and can include interactions between multiple vortices, between vortices and shock waves, and between aircraft components.

An important example of a vortex generator is triangular wings. Interest in these objects is caused by many reasons. Triangular wings have been widely used in aviation since the fifties of the twentieth century. Such aircraft as the Mig 21 and Mirage 3 fighters, which were equipped by the air forces of many countries, are well known. Among aerospace vehicles it is necessary to note, firstly, "Buran" and Space Shuttle. Moreover, different types of interactions are observed for triangular wings: several vortices among themselves, a vortex with a shock wave, and a vortex with a solid surface. All this is of considerable theoretical interest.

Currently, interest in triangular wings in the aerospace industry is increasing due to the development of reusable space systems [1]. Here it is necessary to mention the "Starship" spacecraft [2], the second stage of which has triangular aerodynamic surfaces in the nose and tail parts.

The wide use of triangular wings stimulated active research of their aerodynamics in our country and abroad [3-12].

The earliest attempt to systematize supersonic flows around triangular wings under different flow conditions for different wing geometries was made in [3]. After studying all available experimental data, Stanbrook and Squire proposed a classification of the flow patterns based on the component of the angle of attack normal to the leading edge, α_N, and the component of the Mach number normal to the leading edge, M_N. They divided the flows into two types: attached flow and side-edge breakaway flow. The boundary between these two types exists near $M_N = 1$ and is known as the Stanbrook-Squire boundary. The boundary $M_N = 1$ corresponds to subsonic and supersonic edge modes. In subsequent works, various characteristic flow elements were identified and the classification was considerably complicated taking into account new details. Namely, [9] proposed a classification of flows into six types depending on α_N and M_N, namely (I) classical vortex, (II) vortex with shock wave, (III) detachment bubble with shock wave, (IV) detachment induced by shock wave, (V) shock wave without detachment and (VI) detachment bubble without shock wave. In [10], a similar classification is proposed for much thicker wings. In [11, 12], new details of the flow were found and a classification of the modes was performed. The main features of the flow on the leeward side of the wing in a wide range of values $M_N < 0.8$ are a vortex shroud (primary vortex) coming off the sharp leading edges of the wing, which folds into a pair of main vortices above, below, and between which possibly internal shock shafts appear. The flow, coming off the leading edges, joins along some line, which is the spreading line. The joining of the flow causes an increase in pressure at the point of joining. Under the region of the main vortex, a zone of reduced pressure is formed. The rarefaction peak corresponds to the projection of the nucleus of the main vortex on the wing plane. As the angle of attack increases, the intensity of the main vortex increases, and the rarefaction on the leeward side of the wing increases. An unfavorable pressure gradient (pressure increase between the rarefaction peak and the leading edge) may be sufficient to detach the boundary layer along the stack line. A secondary flow detachment (secondary vortex) occurs. Its attachment occurs along the line of spreading. The distribution of pressure over the wing surface is much less affected by the secondary detachment. As a rule,

the local pressure minimum under the secondary vortex and the pressure maximum corresponding to the joining line are weakly expressed.

Active research of vortex structures formed during the streamline of aerospace vehicles, in fact, led to the formation of a special field of aerodynamics - aerodynamics of concentrated vortex structures [13, 14].

As can be seen from the presented brief review, the flow properties directly above the leeward side of the triangular wing are quite well studied. As for the evolution of the vortex system at a distance from the wing, there are still many open questions, although there are publications on the interaction of the main vortex with the shock wave at the trailing edge. The question of the influence of this vortex structure on the streamline of downstream structural elements requires special attention. In [15] for subsonic flow (velocities of 50 m/s and 60 m/s), numerical and experimental research of the effect of the shaft generated by a triangular wing on the streamline of a downstream sweep wing was carried out. Dependences of aerodynamic coefficients on the height of the vortex trace above the wing are obtained. Signs of flow detachment on the sweep wing under the action of the vortex trace are revealed. These results are undoubtedly of great interest. However, the transfer of subsonic flow properties to supersonic regimes requires special research.

In this work, vortex systems formed in supersonic flow (at Mach number of the onrushing flow M = 2, 3 and Reynolds number Re= 1×10^7 corresponding to a linear dimension of 1 m) of a triangular wing with sharp edges and a sweep angle of 78° [12] are investigated. The influence of Mach number and angle of attack on the intensity of vortices and the position in space of their axes is studied. The influence of the vortex system of a triangular wing on the flow of a rectangular wing located at some distance downstream from the trailing edge of the triangular wing is considered.

PROBLEM STATEMENT

To research the problem, we considered supersonic flow of a triangular wing with sharp edges and sweep angle χ= 78°. The length of its root chord was b_0 = 0.526 m, half span 0.1118 m.

Fig. 1 shows the scheme of the computational domain: a) for the problem of the triangular wing flow considered in the first part of the paper, b) for the problem of the influence of the vortex system of the triangular wing on the rectangular wing flow considered in the second part of the paper.

In numerical calculations, unstructured meshes consisting of curvilinear hexahedra were used. For the first problem, the number of cells was of the order of 7.5 million, for the second of the order of 12.5 million.

The calculation is performed in a coupled coordinate system. In the counting domain, a Cartesian coordinate system was defined, the origin of which coincides with the apex of the triangular wing; the $O_x$axis is directed along the root chord, O_z is perpendicular to the plane of symmetry. The midface of the wing lies in the plane z= 0. At the considered Mach numbers M= 2, 3 the normal Mach number $M_N = M \cos(\chi)$ takes values 0.416 and 0.624 respectively, i.e. the leading edge is subsonic.

Numerical data were obtained using the author's ARES [16] software package [16] for calculating three-dimensional turbulent flows of viscous compressible gas, which was developed and programmatically implemented at the Keldysh Institute of Mathematics and Mathematics of the Russian Academy of Sciences. The mathematical model and numerical algorithm are described in more detail in [17].

Numerical calculations were performed on the hybrid supercomputer system K-60 [18] at the Keldysh IPM Center of the Russian Academy of Sciences using 196 processors.

In the considered range of Mach numbers and angles of attack, the vortex system consists of the following main elements. A side edge vortex (primary vortex), a main vortex and a secondary vortex are formed above the leeward side of the wing - Fig. 2. This figure shows the distribution of the x component of the rotor velocity (swirl) Ω_x (*X Vorticity*) and the current lines in the x= 0.45 cross section crossing the wing near the trailing edge. The secondary vortex is caused by the detachment of the boundary layer, which is due to the pressure rise towards the trailing edge. The secondary vortex has a direction of rotation opposite to that of the main vortex.

EFFECT OF ANGLE OF ATTACK ON VORTEX SYSTEM PARAMETERS

We consider the flow of a triangular wing at Mach number of the oncoming flow M = 2 and angles of attack α = 10° and α = 20° (the angle between the vector of velocity of the oncoming flow and the *Ox* axis).

Fig. 2 shows that the vortex region at α = 20° has slightly larger dimensions than at α = 10°. Moreover, for α = 20°, the vortex axis is located at a greater distance from the wing surface and closer to the plane of symmetry. The latter fact will be further illustrated in the following figures. The general view of the vortex systems in space for two variants of the angles of attack

is shown in Fig. 3, where the isosurface of the velocity (vorticity) rotor modulus *Vort* = 100 is shown. It can be seen that the main vortex becomes wider as the angle of attack increases.

As shown by earlier research, in many cases the axis of the main vortex is quite well identified as a 3D line on which the pressure minimum is reached in cross sections $x = const$. This fact is also confirmed by the results of other authors, for example [19]. The line of minimum density corresponds to the axis of the secondary vortex. The vortex at the edge is represented by the line of maximum vorticity. In Fig. 4, the position of the vortex axes in space is shown for the variant M = 2, $\alpha = 10°$.

As can be seen in Fig. 4, the secondary and vortex axes at the lateral edge undergo significant deformations in the region behind the wing. At some distance downstream, all axes practically merge. The transformation of the vortex system is caused by the shock wave at the trailing edge of the wing.

Fig. 5 shows the distribution of pressure and vorticity near the trailing edge in the plane passing through the axis of the main vortex. The problem of the interaction between a supersonic vortex and an inclined jump has been sufficiently well investigated to date [20-22]. In particular, in [20] it is shown that the type of interaction (weak, moderate, strong) is largely determined by the deficit of the longitudinal velocity V_x/V_∞ along the vortex axis. At the axis of the main vortex, the velocity is sufficiently large (even exceeds the velocity of the onrushing flow). Therefore, a weak type of interaction with the shock wave is realized for the main vortex, in which the vortex and the shock wave undergo insignificant changes. For the secondary vortex and the edge vortex, the velocity deficit is 0.05 and 0.43, respectively. A strong type of interaction with almost complete destruction of the vortex and significant deformation of the shock wave surface is realized.

The effect of the angle of attack on the vortex system is illustrated in Fig. 6, which shows the axes of the main vortex in projection on the *xOy* and *xOz* planes. It can be seen that for both modes, the angles of inclination of the axes in the *xOy* plane increase under the influence of the shock wave. The axis of the main vortex is located much higher at a larger angle of attack. The distance between the axes in the vertical direction increases with distance from the wing. In the *xOz* plane, there is also a sharp change in the angles of the axes under the action of the shock wave. After the interaction, the distance from the plane of symmetry in the transverse direction increases very slowly away from the wing. As already mentioned in the analysis of Fig. 2, the axis of the main vortex at $\alpha = 20°$ is located somewhat closer to the plane of symmetry.

Table 1 presents in Table 1 the aerodynamic coefficients C_d, C_l in the velocity coordinate system. The first column shows the friction resistance coefficient C_{df}. As can be seen, the

contribution of the friction force to the total resistance does not exceed 11%. It can also be noted that the friction resistance changes insignificantly when changing the angle of attack, so the observed change in aerodynamic coefficients is mainly due to the action of pressure forces.

For a rectangular wing in an incompressible flow, there is a simple linear relationship between the lift force and the intensity (circulation) of the vortex system [23, 24]. For the considered case of supersonic flow of a triangular wing, the issue is much more complicated [14, 25, 26], however, a dependence close to linear is observed. When the angle of attack increases by a factor of 2 (from 10° to 20°), the coefficient C_y (in the coupled coordinate system) increases by a factor of 2.1. At the same time, the normalized (normalized by the velocity of the oncoming flow) integral of the longitudinal shaft of the rotor velocity $\int \Omega_x dS / M\sqrt{\gamma}$ in section $x = 1.2$ increases modulo 2.2 times, Table 2.

As can be seen in Fig. 7, which shows the pressure distribution in the cross section $x = 1.2$, the main shafts are clearly localized as low-pressure regions. At the same time, as in Fig. 6, it can be seen that at $\alpha = 20°$ the vortex is located much higher than at $\alpha = 10°$.

INFLUENCE OF MACH NUMBER ON VORTEX SYSTEM PARAMETERS

In this part of the paper, the flow of a triangular wing is considered at angle of attack $\alpha = 14°$ (the angle between the velocity vector of the oncoming flow and Ox) and Mach numbers of the oncoming flow M = 2 and M = 3.

When the Mach number changes in the considered range, the main structure of the flow remains the same as described in the previous section. It contains structure-forming vortices: main, secondary, and trailing edge vortices. As the Mach number increases, the axes of these structure-forming vortices behind the wing merge closer to the trailing edge of the wing.

It is found that the main vortex continues far beyond the wing tip in the form of a distinct structure. For the flow with M = 3, the vortex structures undergo slightly larger perturbations.

Fig. 8 shows the axes of the main vortex in projection on the xOy and xOz planes, the change in the position of which illustrates the effect of Mach number on the vortex system. Thus, with increasing Mach number, the y coordinate changes insignificantly and there is a small shift of the main vortex axis position mainly along the z coordinate. As Mach number increases, the vortex axis is located somewhat closer to the plane of symmetry. At the same time, the axis inclination angle remains practically unchanged with increasing Mach number.

Presented in Table 3 are the aerodynamic coefficients (in the velocity coordinate system) at different Mach numbers of the incoming flow for the wing at the angle of attack $\alpha = 14°$. As in the research on the effect of attack, a close to linear relationship between the lift force and

the intensity of the vortex system can be traced. When Mach is increased by a factor of 1.5 (from 2 to 3), the coefficient C_y decreases by a factor of 1.3, and the coefficient $C_x$increases by a factor of 1.26. Simultaneously, the integral of the longitudinal shaft of the normalized rotor velocity $\int \Omega_x dS / M\sqrt{\gamma}$ in the presented sections along x (Table 4) decreases modulo 1.25 times.

It is very important to note that the value of $\int \Omega_x dS / M\sqrt{\gamma}$ varies very slightly from section to section, which indicates a rather weak manifestation of dissipative effects (Table 4). Moreover, the data in Tables 3 and 4 show that, as for the above discussed effect of the angle of attack of the wing, the dependences in supersonic flows are much more complicated than for incompressible flows. In particular, in this case, the following effect is observed: as Mach number M increases, the integral of the longitudinal shaft of the normalized velocity rotor decreases modulo the lift coefficient.

Figure 9 shows the pressure distribution in cross section x = 1.2 at M = 2 (left) and M = 3 (right), α = 14°. The main vortices in the x = 1.2 cross section (Fig. 11) are clearly localized as low-pressure regions, as in the previous section. It can also be noted that for lower Mach number the structure (pressure distribution) of the vortex trace is more homogeneous.

It is found that as the Mach number of the impinging flow increases, the vortex becomes wider and the influence of the tail jump on the vortices increases.

INFLUENCE OF THE VORTEX SYSTEM OF A TRIANGULAR WING ON THE FLOW OF A DOWNSTREAM RECTANGULAR WING

In the previous sections, it was shown that the vortex system of a triangular wing extends to quite large distances from its trailing edge. Therefore, the question arises about its influence on downstream elements of the aircraft structure.

To research this problem, a rectangular wing with sharp edges and a diamond-shaped profile, a chord of 0.045 m and a half-span of 0.12 m was placed at a distance of 0.5 of its chord from the trailing edge of the triangular wing (Fig. 1b). The midline was raised to a height of 0.124 of the root chord of the triangular wing with respect to the triangular wing. The rectangular wing had chord and half span. Streamline regimes were considered at M = 2, M = 3 and Reynolds number Re = 1×10^7 (corresponding to a linear dimension of 1 m), with angle of attack α = 14°.

The interaction of the vortex system with a rectangular wing is presented in Fig. 10, which shows the isosurfaces of the longitudinal component of the *X Vorticity*. The primary vortex intersects with the wing surface. The primary vortex intersects with the wing near the lateral edge and influences the formation of the end vortex. Some distance downstream of the

rectangular wing, its end vortex and the deformed main vortex of the triangular wing remain. These two vortices have the same directions of rotation. The formation of secondary vortices of opposite rotation direction is also observed.

The formation of secondary shafts can also be seen in Fig. 11, which shows the distribution of rotor modulus in the $x = 0.785$ cross section located at a distance of 22% of the chord from the trailing edge of the rectangular wing upstream.

Secondary vortices are formed by detachment of the boundary layer on both the lower and upper surfaces of the wing.

The presence of the shaft system of the triangular wing causes the rectangular wing to be streamlined by a very inhomogeneous flow, which is illustrated in Figs. 12 and 13, which show the properties of the flow impinging on the rectangular wing in its immediate vicinity.

In particular, we note the presence of a region of high Mach number in the vicinity of the cross section $z = 0.5$, which itself could lead to an increase in pressure on the wing surface. However, there is also a region of low pressure here. Therefore, the overall effect will be quite complex and the general scheme of the flow will be significantly different from the flow of the wing with a uniform flow with the corresponding Mach number and angle of attack. Note, however, that the general perturbation structures for M = 2 and M = 3 are not fundamentally different.

The distribution of pressure on the wing surface for M = 2 is presented in Fig. 14 and Fig. 15. As can be seen, compared to the uniform flow, both underpressure and overpressure zones appear. The total effect on aerodynamic coefficients is presented in Table 5.

As can be seen from the data in tables 5, 6 for M = 2, the resistance coefficient decreases by 38% and the lift coefficient by 40%. At the same time, the aerodynamic quality (K) decreases by 3%. Similarly, for M = 3, the resistance and lift force decrease (Table 6). However, in this case, there is a slight increase in aerodynamic quality - by 1%.

At the considered values of the problem parameters (firstly, the relative position of the wings) for M = 2 we can speak about the negative influence of the vortex system - some reduction of the aerodynamic quality. This fact is important if the rectangular wing is considered as a bearing surface of an aircraft. If the rectangular wing is a control organ, the fact of normal force reduction has independent importance.

VALIDATION

Testing of the algorithm and program was performed on the basis of comparison with experimental data [12] for the regime M = 2, $\alpha = 14°$ (Fig. 16). It is noted in [12] that in the

considered flow regimes, the local pressure minima on the leeward surface of the wing are located under the vortices (main and secondary).

As can be seen in Fig. 16, the numerical data obtained show good agreement with the experimental data, in particular the position of the main and secondary shafts and their influence on the pressure distribution.

CONCLUSIONS

In this paper, a vortex system formed behind a triangular wing in supersonic flow is investigated. The dependence of the formed vortex structures on the angle of attack of the triangular wing and on the Mach number of the incoming flow is obtained. Their influence on the aerodynamic properties of a straight wing located downstream is investigated.

As the angle of attack increases, the main vortex diameter increases and its axis is displaced farther from the wing surface and closer to the plane of symmetry; the angle of inclination of the main vortex along the *y-axis* also increases. The *y-coordinate* of the main vortex axis changes insignificantly with increasing Mach number of the incoming flow, but there is a small displacement of its *z-coordinate*.

The question of the dependence between the lift force and the intensity (circulation) of the vortex system is much more complicated for the considered supersonic flow than for incompressible flow, however, a dependence close to linear, is observed. Indeed, when the angle of attack increases by a factor of 2 (from 10° to 20°), the normal force coefficient increases by a factor of 2.1. At the same time, the normalized integral of the longitudinal component of the rotor velocity in section x = 1.2 increases modulo 2.2 times. At growth of Mach number of the onrushing flow in 1.5 times (from 2 to 3) the normal force coefficient decreases in 1.3 times. At the same time, the integral of the longitudinal component of the normalized velocity rotor decreases in modulus by a factor of 1.25, i.e., approximately as the normal force coefficient. Further research of these dependences is planned.

The general picture of interaction between the vortex system of a triangular wing and a downstream rectangular wing is revealed. The analysis shows that all elements of the vortex system (primary vortex, main vortex, secondary vortex) have a certain influence on the wing flow. The primary vortex intersects with the wing surface and influences the distribution of pressure on it. The primary vortex intersects with the wing near the lateral edge and influences the formation of the end vortex. Some distance downstream of the rectangular wing, its end vortex and the deformed primary vortex of the triangular wing remain. These two vortices have

the same rotation directions. The formation of secondary vortices of opposite rotation direction is also observed.

At the considered values of the problem parameters, a significant effect of the vortex system of the triangular wing on the aerodynamic characteristics of the straight wing is recorded. For both M = 2 and M = 3, a decrease in resistance and lift is observed. The magnitude of this reduction is of the order of 38% and 40%, respectively, for M = 2, of the order of 29% and 28%, respectively, for M = 3. Further research on this effect is needed for practical applications, in particular for other variants of the relative positioning of the vortex generator and the main wing.

FUNDING

This work was financially supported by the Russian Science Foundation, project No. 24-21-00230.

REFERENCES

1. *Dietlein I., Bussler L., Stappert S., Wilken J., Sippel M.* Overview of system study on recovery methods for reusable first stages of future European launchers // CEAS Space J (2024). https://doi.org/10.1007/s12567-024-00557
2. Internet resource https://www.youtube.com/watch?v= j2BdNDTlWbo
3. *Stanbrook A., Squire L. C.* Possible types of flow at swept leading edges // Aeronaut. Quart. 1964. V. 15, N. 2. P. 72-82.
4. *Bashkin B.A.* Experimental research of flat triangular wings streamline at number M = 5 in the range of angles of attack from 0 to 70° // Izv. of the USSR Academy of Sciences. MZHG. 1967. № 3. P. 102-108.
5. *Squire L.C.* Flow regimes over delta wings of supersonic and hypersonic speeds // Aeronaut Quart. 1976. V. 27, N. 1. P. 1-14.
6. *Borovoy V.Ya., Ivanov B.A., Orlov A.A., Kharchenko V.N.* Research methods of the supersonic flow streamline of wings of different shape in plan view by the laser knife method // Proceedings of TsAGI. 1977. Issue. 1793.
7. *Keldysh V.V., Lapina N.G.* Experimental research of the flow in the vicinity of triangular wings with a sharp and rounded leading edge at supersonic speeds // Proceedings of TsAGI. 1980. Issue. 2074.
8. *Maikapar G.I.* Detachment currents at the leeward side of a triangular wing and a body of rotation in a supersonic flow // Scientific Notes of TsAGI. 1982. V.13. № 4. P. 22-33.

9. *Wood R.M., Miller D.C.* Lee side flow over delta wings at supersonic speeds // J. Aircraft. Aircraft. 1984. V. 21. P. 680-686.
10. *Szodruch J.G., Peake D.J.* Leeward flow over delta wings at supersonic speeds // Rep. NASA TM. 1980. N. 81187.
11. *Seshadri S.N., Narayan K.Y.* Possible types of flow on lee-surface of delta wing at supersonic speeds // Aeronaut. J. 1988. N. 5. P. 185-199.
12. *Brodetsky M.D., Krause E., Nikiforov S.B., Pavlov A.A., Kharitonov A.M., Shevchenko A.M.* Development of vortex structures on the leeward side of a triangular wing (in Russian) // PMTF. 2001. V.42. № 2. P. 68-80.
13. *Alekseenko S.V., Kuibin P.A., Okulov V.L.* Introduction to the theory of concentrated vortices. Institute of Computer Research, 2005. 503 p. ISBN 5-93972-397-7.
14. *Luckring J.M., Rizzi A.* Prediction of concentrated vortex aerodynamics: Current CFD capability survey // Progress in Aerospace Sciences. 2024. V. 147. 100998. https://doi.org/10.1016/j.paerosci.2024.100998
15. *Voevodin A.V., Sudakov G.G., Shapovalov G.K.* Vortex diffraction on a sweep wing // Fluid and Gas Mechanics. 1998. №6. P. 98-105.
16. *Borisov V.E., Davydov A.A., Kudryashov I.Yu., Lutskiy A.E.* Program complex ARES for calculation of three-dimensional turbulent flows of viscous compressible gas on high-performance computing systems. // Certificate of registration of the program for computer RU 2019667338. 23.12.2019.
17. *Borisov V.E., Konstantinovskaya T.V., Lutskiy A.E.* Numerical modeling of the influence of supersonic vortex structures on the heat transfer on the bearing surfaces of aircraft // Izv. RAS. MZHG. 2024. № 5. P. 86-95.
18. K-60 Computing Complex. https://www.kiam.ru/MVS/resourses/k60.html
19. *Holzäpfel F., Misaka T., Hennemann I.* Wake-Vortex Topology, Circulation, and Turbulent Exchange Processes // AIAA Paper 2010-7992. AIAA Atmospheric and Space Environments Conference, Toronto, Ontario, Canada, August 2-5, 2010, 16 pages.
20. *Zudov V.N., Pimonov E.A.* Interaction of a longitudinal vortex with an inclined shock wave (in Russian) // PMTF. 2003. V. 44. № 4. P. 10-21.
21. *Settles G.S., Cattafesta L.* Supersonic shock wave/vortex interaction. Pen State Univ. 1993. NASA-CR-192917. P. 43.
22. *Magri V., Kalkhoran Iraj M.* Numerical investigation of oblique shock wave/vortex interaction // Computers & Fluids. 2013. 86. P. 343-356.

23. *Golubev A.G., Epikhin A.S., Kalugin V.T., Lutsenko A.Y., Moskalenko V.O., Stolyarova E.G., Khlupnov A.I., Chernukha P.A.;* ed. by V.T. Kalugin. Aerodynamics: textbook for universities. V. T. 2nd edition, revised and supplemented. Moscow: Izd-e vo N.E. Bauman Moscow State Technical University, 2017. 607 p. ISBN: 978-5-7038-4428-1
24. *Gaifullin A.M.* Vortex currents: Nauka, 2015. 319 p. ISBN 978-5-02-039128-4.
25. *Luckring J.M.* The discovery and prediction of vortex flow aerodynamics // The Aeronautical Journal. 2019. V. 123. N. 1264. P. 729-803.
26. *Imai G., Fujii K., Oyama A.* Computational Analyses Of Supersonic Flows Over A Delta Wing At High Angles Of Attack // ICAS 2006, 25th Congress of International council of the Aeronautical Science, 2006, Hamburg, Germany. Paper ICAS2006-2.5S

TABLES

Table 1. Aerodynamic coefficients of triangular wing as a function of angle of attack α at M = 2

α	C_{df}	C_d	C_l	$K = C_l/C_d$
10º	5.721e-003	0.0489	0.2399	4.9066
20º	5.238e-003	0.1807	0.4790	2.6507

Table 2. Value of $\int \Omega_x dS \Big/ M\sqrt{\gamma}$ in section $x = 1.2$

α	$\int \Omega_x dS \Big/ M\sqrt{\gamma}$
10º	-0.0452
20º	-0.1011

Table 3. Aerodynamic coefficients of a triangular wing as a function of Mach number at α = 14 º

M	C_{df}	C_d	C_l	$K = C_l/C_d$
2	5.518×10^{-3}	0.0909	0.3388	3.7259
3	4.803×10^{-3}	0.0809	0.2627	3.2466

Table 4. Magnitude of $\int \Omega_x dS / M\sqrt{\gamma}$ in cross sections $x = 0.7$, $x = 1.2$ and $x = 1.7$

M	$x = 0.7$	$x = 1.2$	$x = 1.7$
2	-0.0689	-0.0682	-0.0674
3	-0.0547	-0.0545	-0.0547

Table 5. Aerodynamic coefficients of a rectangular wing at M = 2, α = 14º

Variant	C_{df}	C_d	C_l	$K = C_l/C_d$
Constant flow	6.289×10^{-3}	0.1776	0.5799	3.2649
Vortex disturbances	5.577×10^{-3}	0.1102	0.3494	3.1694

Table 6. Aerodynamic coefficients of a rectangular wing at M = 3, α = 14º

Variant	C_{df}	C_d	C_l	$K = C_l/C_d$
Constant flow	6.1830×10^{-3}	0.1137	0.3668	3.2253
Vortex disturbances	4.8031×10^{-3}	0.0809	0.2627	3.2466

FIGURE CAPTIONS

Fig. 1. Scheme of the computational domain: triangular wing (a), system of two wings (b).

Fig. 2. Cross section $x = 0.45$. Distribution of longitudinal *X Vorticity*, particle trajectories in projection onto the x plane = *const*. $\alpha = 10°$ (left), $\alpha = 20°$ (right).

Fig. 3. Isosurface (*Vort* = 100) of the velocity rotor module; $\alpha = 10°$ (left), $\alpha = 20°$ (right).

Fig. 4. Axes of vortices: primary (on the lateral edge), main and secondary. M = 2, $\alpha = 10°$.

Fig. 5. Distribution of pressure (left) and vorticity (right) in the plane passing through the axis of the main vortex.

Fig. 6. Coordinates of the main vortex axes in the *xOy* (left) and *xOz* (right) planes.

Fig. 7. Pressure distribution in cross section x = 1.2, α = 10° on the left, α= 20° on the right.

Fig. 8. Coordinates of the main vortex axes in the *xOy* (left) and *xOz* (right) planes for M = 2 and M = 3, α = 14°.

Fig. 9. Pressure distribution in cross section x = 1.2, α = 14°, M = 2 (left), M= 3 (right).

Fig. 10. Vortex system. Isosurfaces of the longitudinal component of the velocity rotor (vorticity). Interaction with a rectangular wing: M = 2 (left), M = 3 (right).

Fig. 11. Curl distribution in cross section x = 0.785: M = 2 (left), M = 3 (right).

Fig. 12. Distribution of Mach number in front of the leading edge (its projection is shown by the white line) of a rectangular wing: M = 2 (left), M = 3 (right).

Fig. 13. Distribution of pressure P in front of the leading edge (its projection is shown by the white line) of a rectangular wing: M = 2 (left), M = 3 (right).

Fig. 14. M = 2. Distribution of pressure P on the leeward side of a rectangular wing. Streamline with uniform flow (right.)

Fig. 15. M = 2. Distribution of pressure P on the windward side of a rectangular wing. Streamline with uniform flow (right).

Fig. 16. Distribution of pressure coefficient in the cross section x/b_0 = 0.433: exp - experimental data [12], SAIDDES - numerical data obtained using the SAIDDES turbulence model.

(a) (b)

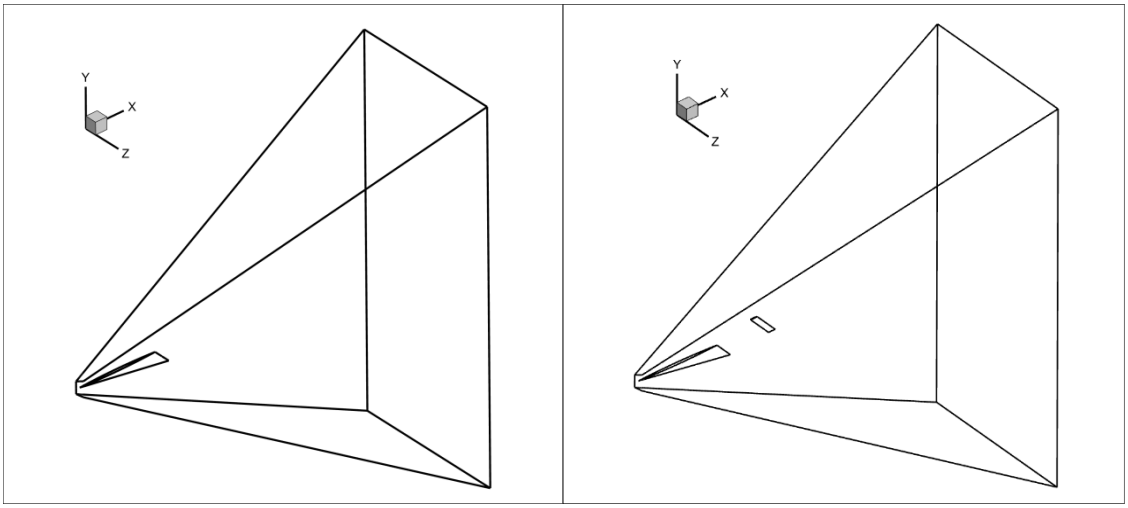
Y
X
Z
Y
X
Z

Fig. 1.

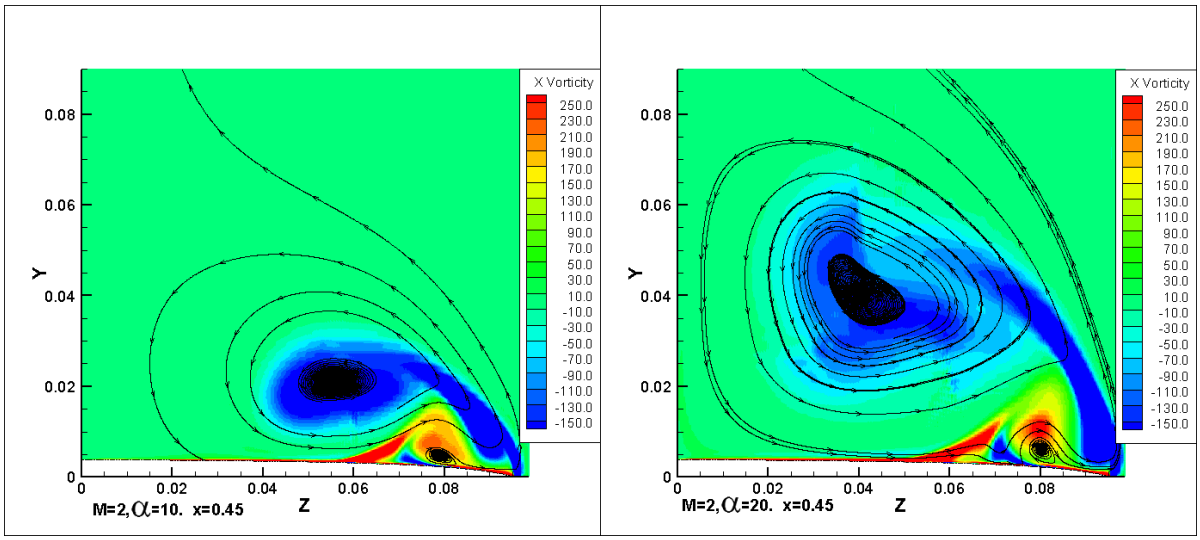
X Vorticity
250.0
230.0
210.0
190.0
170.0
150.0
130.0
110.0
90.0
70.0
50.0
30.0
10.0
-10.0
-30.0
-50.0
-70.0
-90.0
-110.0
-130.0
-150.0
0.08
0.06
0.04
0.02
0
Y
0
0.02
0.04
0.06
0.08
Z
M=2,α=10. x=0.45
X Vorticity
250.0
230.0
210.0
190.0
170.0
150.0
130.0
110.0
90.0
70.0
50.0
30.0
10.0
-10.0
-30.0
-50.0
-70.0
-90.0
-110.0
-130.0
-150.0
0.08
0.06
0.04
0.02
0
Y
0
0.02
0.04
0.06
0.08
Z
M=2,α=20. x=0.45

Fig. 2.

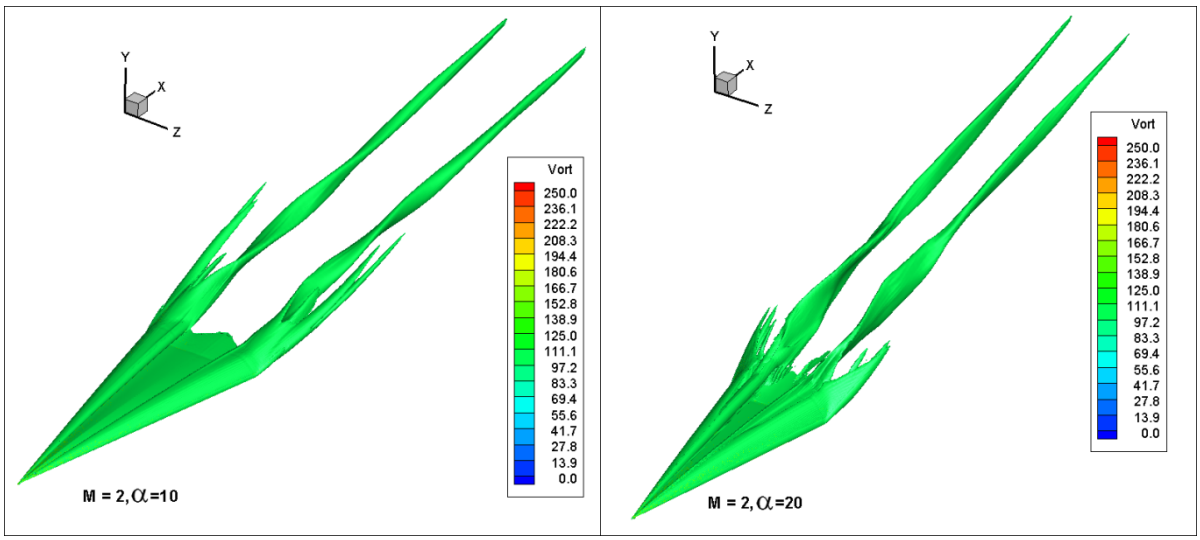
Y
X
Z
Vort
250.0
236.1
222.2
208.3
194.4
180.6
166.7
152.8
138.9
125.0
111.1
97.2
83.3
69.4
55.6
41.7
27.8
13.9
0.0
M = 2, α=10
M = 2, α=20

Fig. 3.

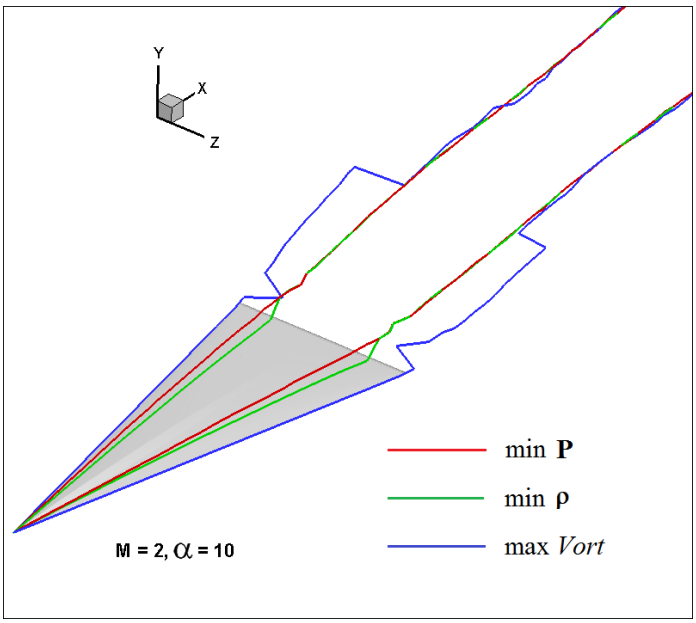
Y
X
Z
M = 2, α = 10
min P
min ρ
max Vort

Fig. 4.

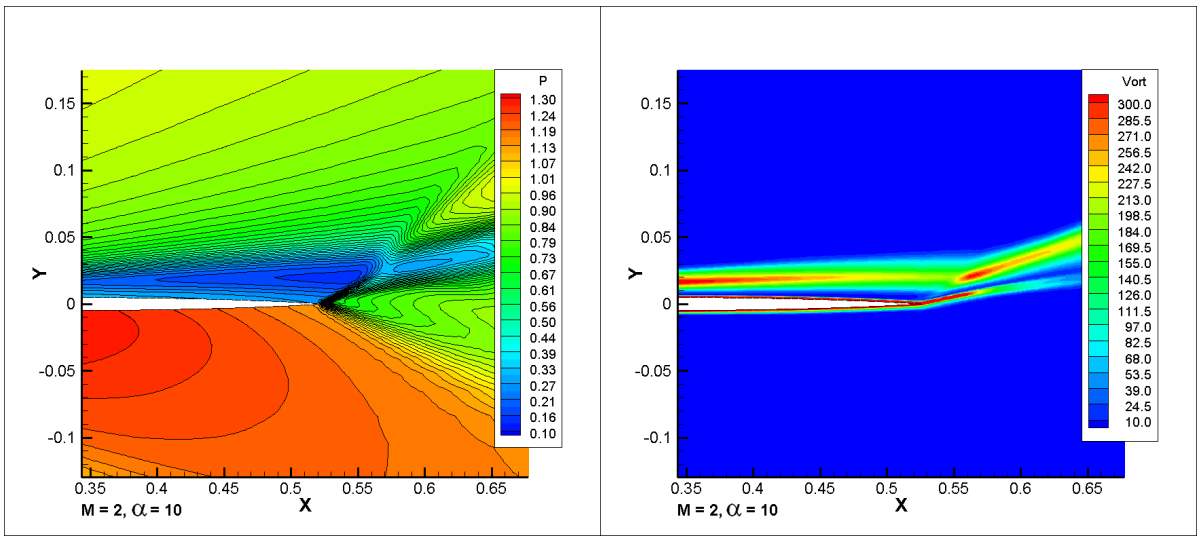
P
1.30
1.24
1.19
1.13
1.07
1.01
0.96
0.90
0.84
0.79
0.73
0.67
0.61
0.56
0.50
0.44
0.39
0.33
0.27
0.21
0.16
0.10
Y
X
M = 2, α = 10
Vort
300.0
285.5
271.0
256.5
242.0
227.5
213.0
198.5
184.0
169.5
155.0
140.5
126.0
111.5
97.0
82.5
68.0
53.5
39.0
24.5
10.0
Y
X
M = 2, α = 10

Fig. 5.

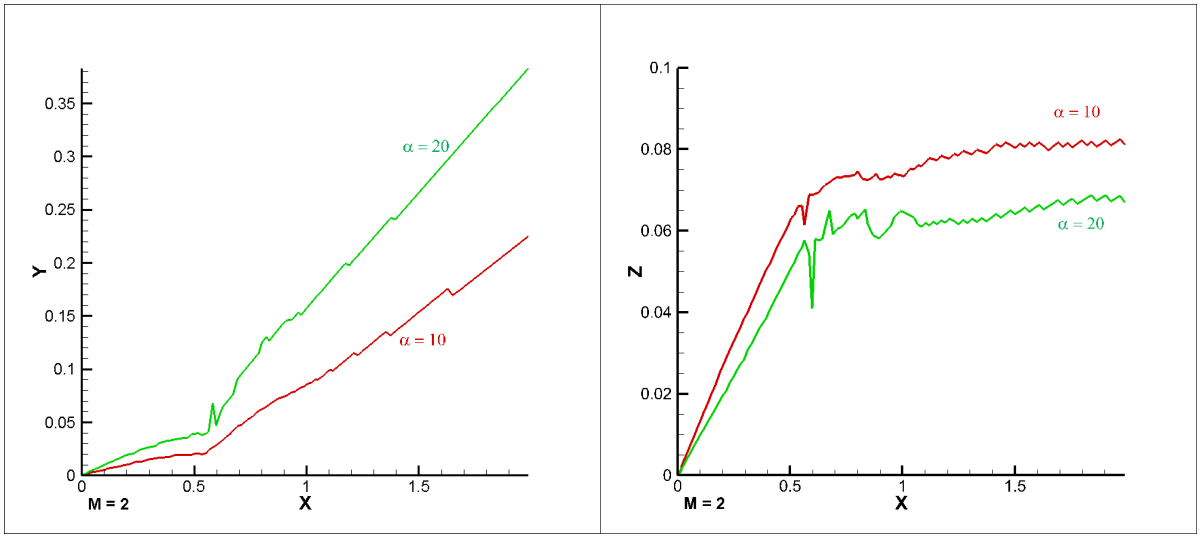
α = 20
α = 10
Y
X
M = 2
α = 10
α = 20
Z
X
M = 2

Fig. 6.

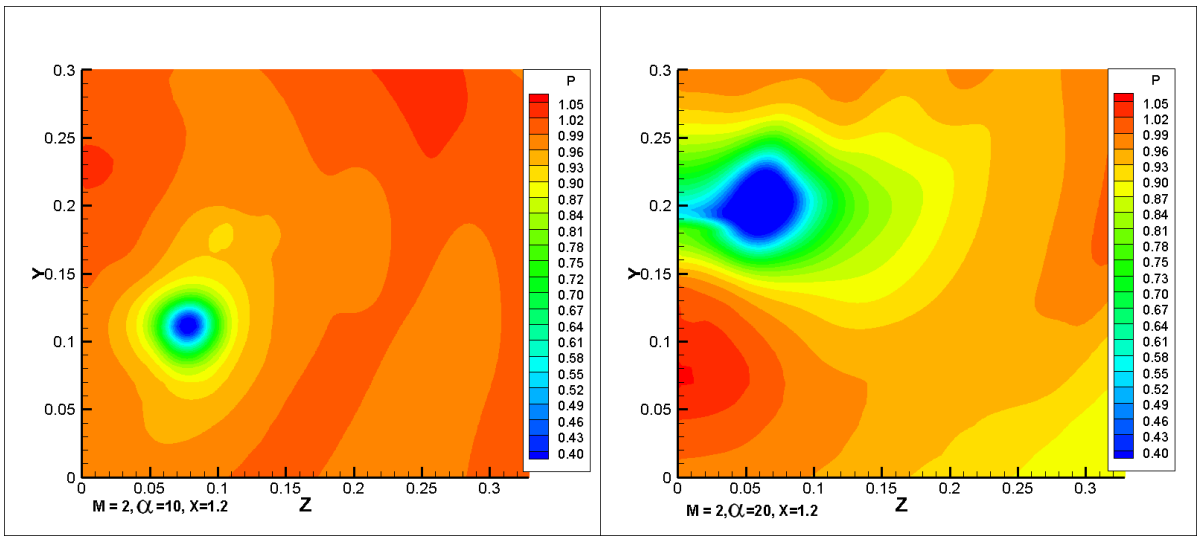
P
1.05
1.02
0.99
0.96
0.93
0.90
0.87
0.84
0.81
0.78
0.75
0.72
0.70
0.67
0.64
0.61
0.58
0.55
0.52
0.49
0.46
0.43
0.40
Y
Z
M = 2, α =10, X=1.2
M = 2,α=20, X=1.2

Fig. 7.

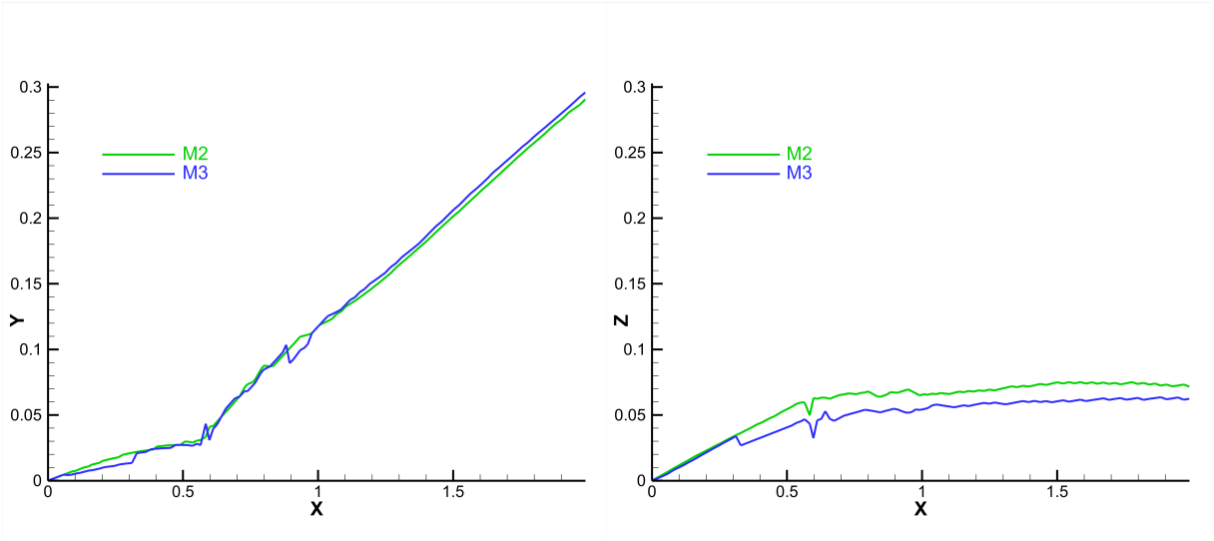
M2
M3
Y
X
Z

Fig. 8.

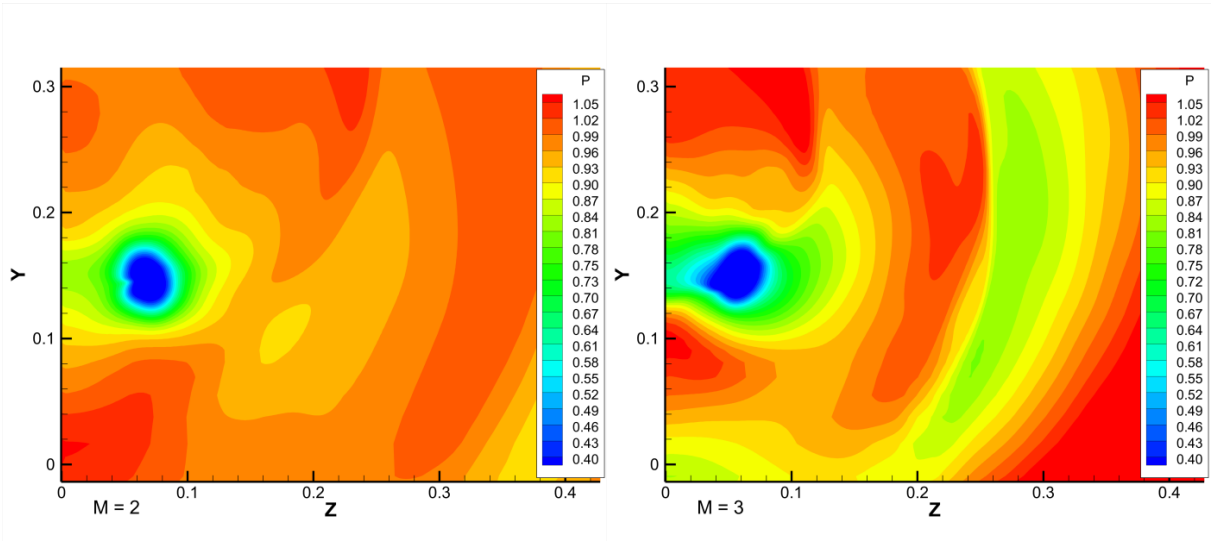
P
1.05
1.02
0.99
0.96
0.93
0.90
0.87
0.84
0.81
0.78
0.75
0.73
0.70
0.67
0.64
0.61
0.58
0.55
0.52
0.49
0.46
0.43
0.40
Y
Z
M = 2
M = 3
0
0.1
0.2
0.3
0.4

Fig. 9.

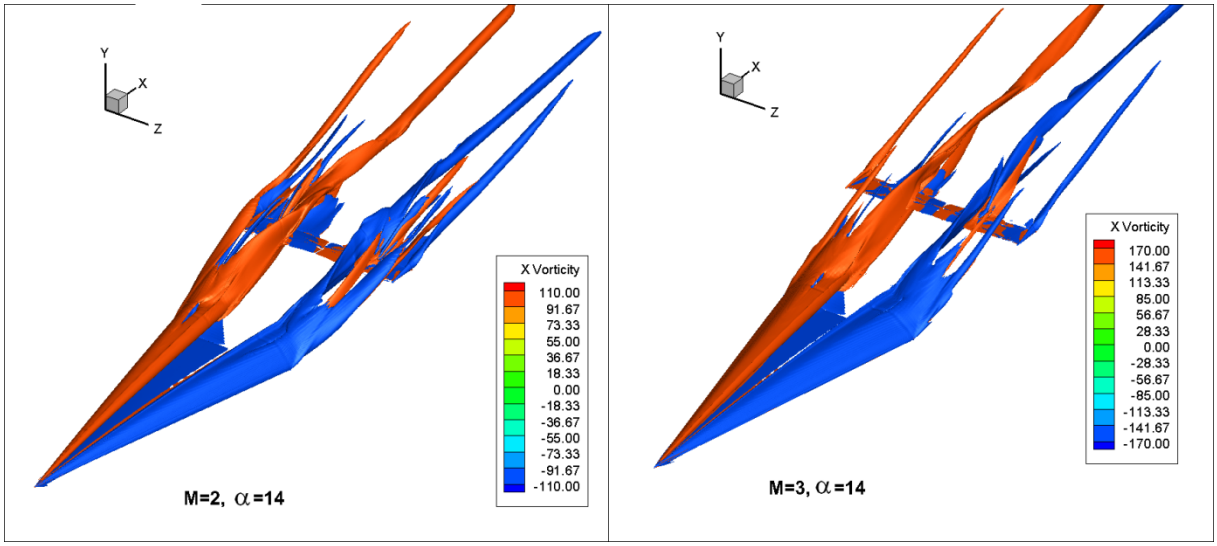
X Vorticity
110.00
91.67
73.33
55.00
36.67
18.33
0.00
-18.33
-36.67
-55.00
-73.33
-91.67
-110.00
170.00
141.67
113.33
85.00
56.67
28.33
0.00
-28.33
-56.67
-85.00
-113.33
-141.67
-170.00
Y
X
Z
M=2, α=14
M=3, α=14

Fig. 10.

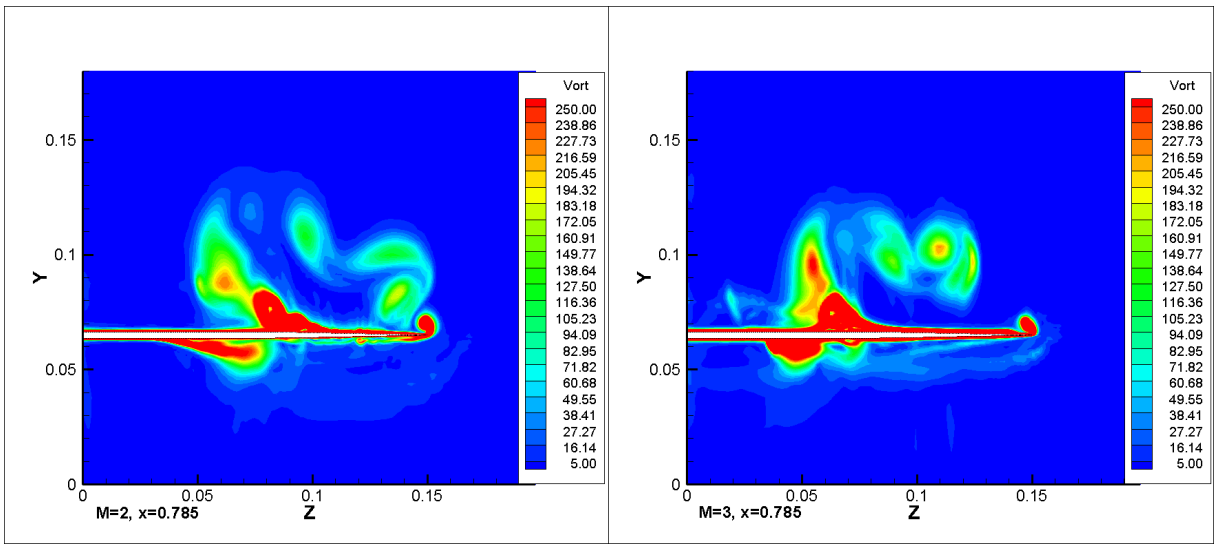
Vort
250.00
238.86
227.73
216.59
205.45
194.32
183.18
172.05
160.91
149.77
138.64
127.50
116.36
105.23
94.09
82.95
71.82
60.68
49.55
38.41
27.27
16.14
5.00
Y
Z
M=2, x=0.785
M=3, x=0.785

Fig. 11.

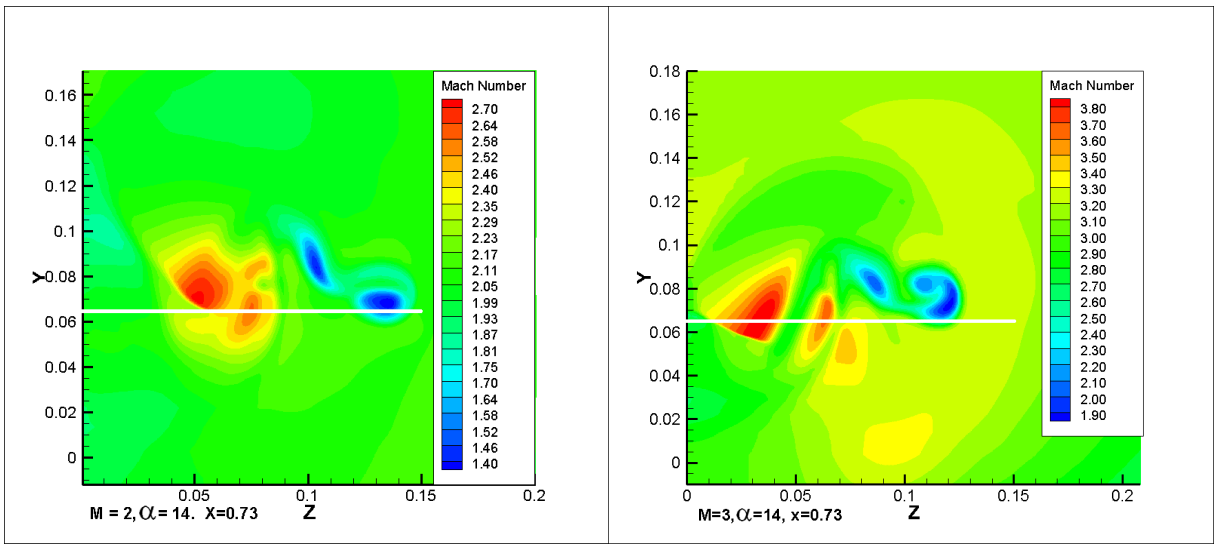
Mach Number
2.70
2.64
2.58
2.52
2.46
2.40
2.35
2.29
2.23
2.17
2.11
2.05
1.99
1.93
1.87
1.81
1.75
1.70
1.64
1.58
1.52
1.46
1.40
3.80
3.70
3.60
3.50
3.40
3.30
3.20
3.10
3.00
2.90
2.80
2.70
2.60
2.50
2.40
2.30
2.20
2.10
2.00
1.90
Y
Z
M = 2, α = 14. X=0.73
M=3, α=14, x=0.73

Fig. 12.

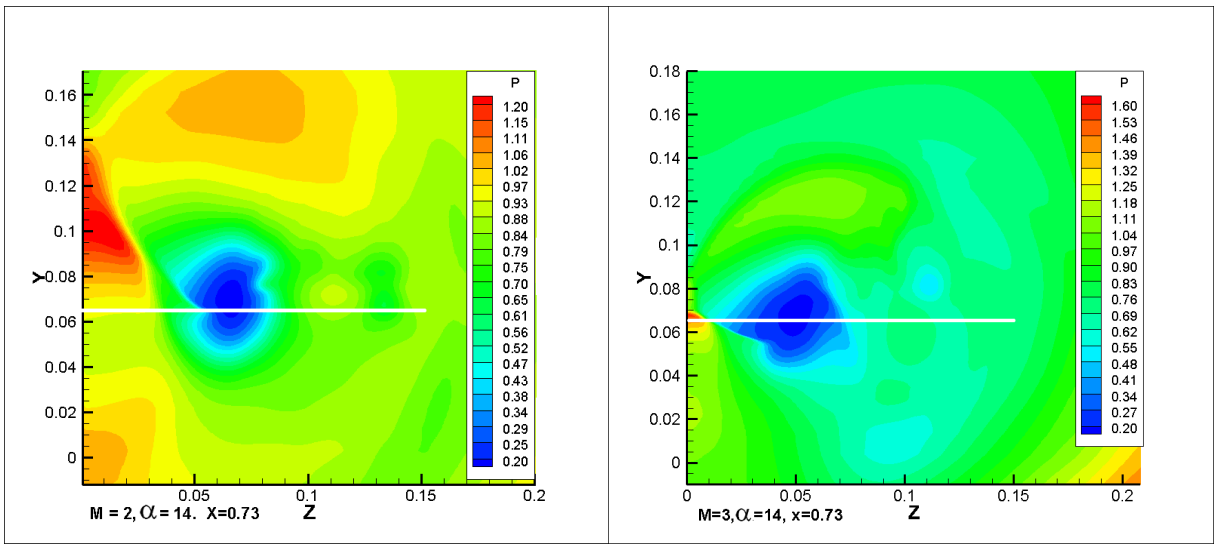
P
1.20
1.15
1.11
1.06
1.02
0.97
0.93
0.88
0.84
0.79
0.75
0.70
0.65
0.61
0.56
0.52
0.47
0.43
0.38
0.34
0.29
0.25
0.20
Y
Z
M = 2, α = 14. X=0.73
P
1.60
1.53
1.46
1.39
1.32
1.25
1.18
1.11
1.04
0.97
0.90
0.83
0.76
0.69
0.62
0.55
0.48
0.41
0.34
0.27
0.20
Y
Z
M=3,α=14, x=0.73

Fig. 13.

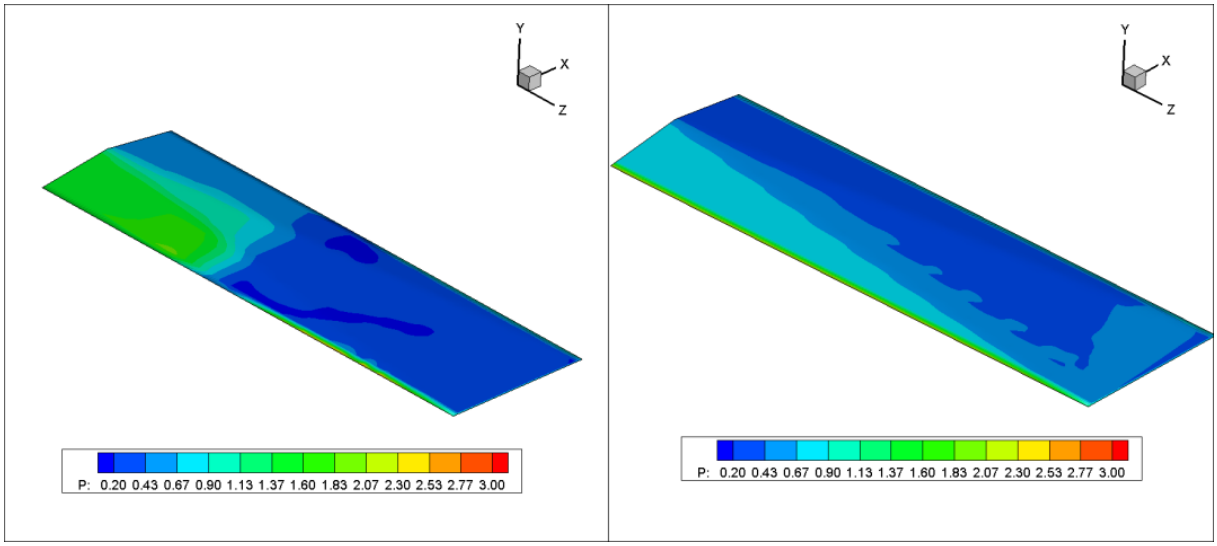
Y
X
Z
P: 0.20 0.43 0.67 0.90 1.13 1.37 1.60 1.83 2.07 2.30 2.53 2.77 3.00
Y
X
Z
P: 0.20 0.43 0.67 0.90 1.13 1.37 1.60 1.83 2.07 2.30 2.53 2.77 3.00

Fig. 14.

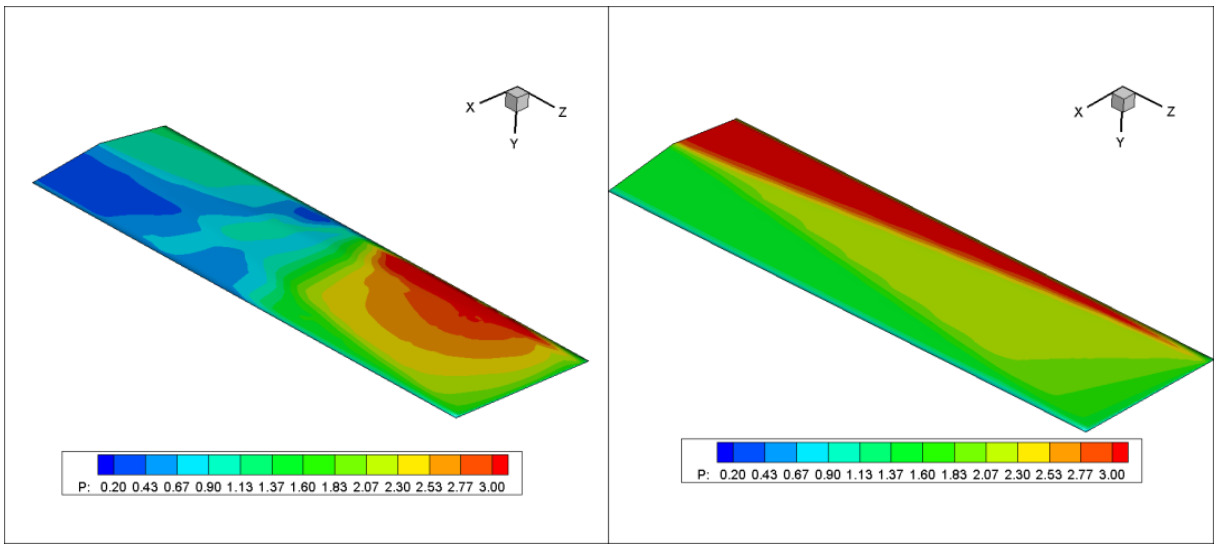
X
Z
Y
P: 0.20 0.43 0.67 0.90 1.13 1.37 1.60 1.83 2.07 2.30 2.53 2.77 3.00
X
Z
Y
P: 0.20 0.43 0.67 0.90 1.13 1.37 1.60 1.83 2.07 2.30 2.53 2.77 3.00

Fig. 15.

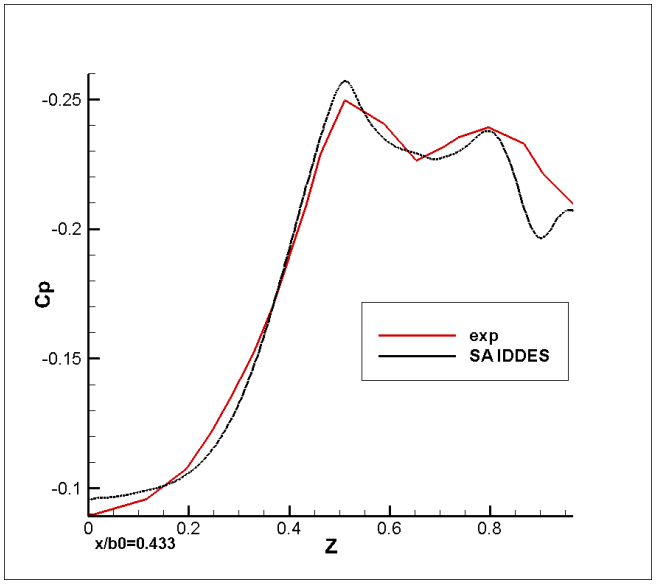
-0.25
-0.2
-0.15
-0.1
Cp
0
0.2
0.4
0.6
0.8
Z
x/b0=0.433
exp
SAIDDES

Fig. 16.